RSC Advances

PAPER

View Article Online
View Journal | View Issue

Cite this: *RSC Adv.*, 2022, **12**, 6732

Effect of unmelted lime on the element distribution behavior on a $CaO–SiO_2–MgO–Al_2O_3–FeO–CaF_2(–Cr_2O_3)$ slag

Qiang Gao [a] and Longhu Cao*[b]

In this study, a $CaO–SiO_2–Al_2O_3–MgO–FeO–CaF_2(–Cr_2O_3)$ slag was chosen according to the compositions of the stainless steel slag for industrial production, and a CaO block was added to the molten slag after the synthetic slag was fully melted. The influences of unmelted lime on the distribution of elements and the structure of product layers at the lime/slag boundary, particularly the existing state of chromium oxide in the chromium-bearing stainless steel slag, were deeply discussed by scanning electron microscopy-energy dispersive spectroscopy (SEM-EDS) and FactSage 7.1. The experiment results indicated that when the unmelted lime existed in the $CaO–SiO_2–Al_2O_3–MgO–FeO–CaF_2$ slag system, two product layers of periclase (MgO) and dicalcium silicate (Ca_2SiO_4) at the boundary of the CaO block were formed. However, when the CaO block was added in the $CaO–SiO_2–Al_2O_3–MgO–FeO–CaF_2–Cr_2O_3$ stainless steel slag, besides MgO and Ca_2SiO_4 product layers, needle-shaped calcium chromite ($CaCr_2O_4$) was also precipitated around the CaO block. Moreover, a small amount of Cr dissolved in the periclase phase. Eh–pH diagrams showed that the $CaCr_2O_4$ and MgO phase unstably existed in a weak acid aqueous solution. Therefore, the existence of unmelted lime in the stainless steel slag could enhance the leachability of chromium.

Received 17th August 2021
Accepted 21st December 2021

DOI: 10.1039/d1ra06226c

rsc.li/rsc-advances

1. Introduction

Significant amount of stainless steel slags are annually produced by the stainless steelmaking companies in China. These slags containing chromium as a heavy metal element are generally accumulated in landfill areas or recycled to harbor construction, road material and civil engineering field. If the existing state of chromium in stainless steel slag is not stabilized, chromium will easily be oxidized to the hexavalent state Cr^{6+} under normal industrial temperature and oxidizing conditions (in air).[1] Simultaneously, Cr^{6+} is known to be highly toxic and carcinogenic, and it is soluble in water and easily migrates into the environment, causing environmental pollution and harm to human health.[2] Moreover, the steel slag is easy to be eroded by rainwater during the storage process, resulting in the leaching of chromium. Therefore, the elution and instability of chromium in stainless steel slag have seriously limited the industrial application of stainless steel slag.[3] In addition, in the production process of stainless steels, a certain amount of lime is added into the molten slag to guarantee the basic melting conditions of the slag, and then achieve the dephosphorization and desulfurization of the molten steel.[4] However, the lime in the molten slag easily react with SiO_2 on the surface to form a dicalcium silicate phase, which prevents the lime from dissolving in the molten slag.[5–8] As a result, a certain amount of unmelted lime still exists in the slag, which affects the existing state of chromium in the slag. Numerous studies on the effect of slag compositions on the stabilization of chromium in stainless steel slag have been investigated by means of modification treatments.[9–12] Nevertheless, research on the influence of unmelted lime on the existing state of chromium oxide in the stainless steel slag and environment are rarely conducted.

In this study, the $CaO–SiO_2–Al_2O_3–MgO–FeO–CaF_2(–Cr_2O_3)$ slag was chosen according to the compositions of the stainless steel slag for industrial production. In order to clarify the action mechanism of the unmelted lime phase in stainless steel slag, the effect of the unmelted lime on the distribution of elements and the structure of product layers in the experimental slags was investigated. The influence of components of slag on the existing state of chromium was systematically analyzed, so as to provide data support for the harmless treatment of stainless steel slag in the further research.

2. Experimental

Based on the composition of field stainless steel slag, the synthetic stainless steel slags were prepared by different reagents. The basicity (*i.e.*, CaO/SiO_2 mass ratio) was designed as 1.5, 3.0% CaF_2 was added to the slag for decreasing the melting temperature, the mass fractions of MgO, Al_2O_3, and

[a]*Shandong University of Technology, China*
[b]*WISDRI Engineering & Research Incorporation Limited, China*

FeO were fixed at 9.0%, 4.0%, and 3.0%, respectively. To conduct the element migration behavior of chromium-contained steel slag, the mass fractions of Cr_2O_3 were designed as 0 and 5.0%, as shown in Table 1. Each experimental sample of 30 g was prepared by chemical reagents of CaO, SiO_2, MgO, Al_2O_3, $FeC_2O_4 \cdot 2H_2O$, Cr_2O_3 and CaF_2 with high purity. Powders of these reagents were weighed precisely, and mixed thoroughly. The mixtures were placed in a molybdenum crucible, which was placed into the constant-temperature zone of the high-temperature tube furnace shown in Fig. 1. Before the experiment, the B-type thermocouple had been calibrated using the standard calibration method, and its accuracy was ±1 K. In the process of a constant temperature, the controlling temperature accuracy was less than ±2 K. High quality argon entered from the bottom of the furnace to protect the slag samples from being oxidized. The mixtures were melted at 1873 K for 30 min to a full melting state. After melting down, the CaO block, which was used to simulate the unmelted lime phase, was added to the molten slag using a molybdenum rod. After 20 min, the samples were quickly taken out from the high-temperature tube furnace and cooled under air atmosphere. The cooled samples were polished carefully, and then, the distribution of elements and the structure of product layers at the lime/slag boundary were obverted and analyzed by scanning electric microscope-energy dispersive spectroscopy (SEM-EDS; Hitachi S3400N, Japan). In addition, an X-ray diffraction analyzer (XRD; PW3040, K_α-Cu) was used for the phase composition analysis with a measuring range of 5–90°, and the solubility of chromium-bearing mineral phases in an aqueous solution was evaluated by FactSage 7.1. In order to analyze the influence of the unmelted lime on the stability of chromium in stainless steel slag, each sample of 10 g was crushed to fine powder with the size less than 74 μm for the leaching test. According to Chinese Waste Norms (HJ/T299-2007), the fine powder was contacted with acid solution of 100 ml at pH 3.2 at 23 ± 2 °C under rotation with 30 rpm for 18 h. The chromium present in the leachate was determined by inductively coupled plasma optical emission spectrometry (ICP-OES).

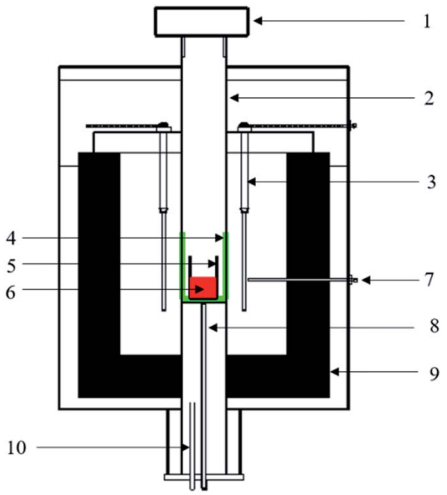

Fig. 1 Schematic of the high-temperature tube furnace. (1) Sealing cover, (2) alumina tube, (3) $MoSi_2$ heater, (4) graphite crucible, (5) Mo crucible, (6) sample, (7) controlled thermocouple, (8) measured thermocouple, (9) refractory bricks, (10) argon inlet.

3. Results and discussion

3.1. Structure of product layers at lime/slag boundary

Fig. 2 shows the SEM images of the dissolution boundary of the S1 sample with a reaction time for 20 min. Two different product layers at the boundary between the unmelted lime and the bulk slag can be observed clearly. The thickness of one product layer near the unmelted lime was approximately 10 μm, and the thickness of the other one near the bulk slag was 60–80 μm. A line-scanning study by EDS was carried out to obtain the concentrations of Ca, Mg, Si and Al elements along the normal direction from the unmelted lime, lime/slag boundary to the bulk slag, as shown in Fig. 3. It can be seen that in the product layer near the unmelted lime, the concentration of Mg element increased abruptly, and the concentrations of Ca, Si and Al elements were almost absent, which revealed that the product layer near the unmelted lime was the Mg-rich region; in the product layer near the bulk slag, the concentration of Mg element was very low, and Ca and Si enrichment zone can be seen evidently between the Mg-rich region and the bulk slag phase.

7 different points were chosen along the normal direction from the unmelted lime, lime/slag boundary to the bulk slag in Fig. 2, and the composition of each point was determined by EDS. The results are listed in Table 2. According to the EDS analysis, point 1 represents the unmelted lime, and points 6–7 represent the bulk slag. Simultaneously, the composition of

Table 1 Chemical composition of synthetic stainless steel slags (mass, %)

Sample	CaO	SiO_2	MgO	Al_2O_3	FeO	Cr_2O_3	CaF_2	Basicity
S1	48.6	32.4	9.0	4.0	3.0	0	3.0	1.5
S2	45.4	30.6	9.0	4.0	3.0	5.0	3.0	1.5

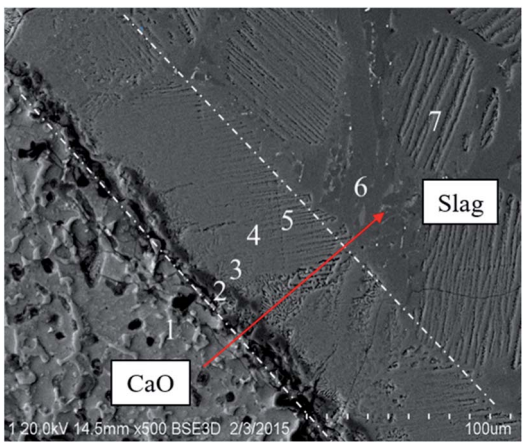

Fig. 2 SEM for the S1 sample at the lime/slag boundary.

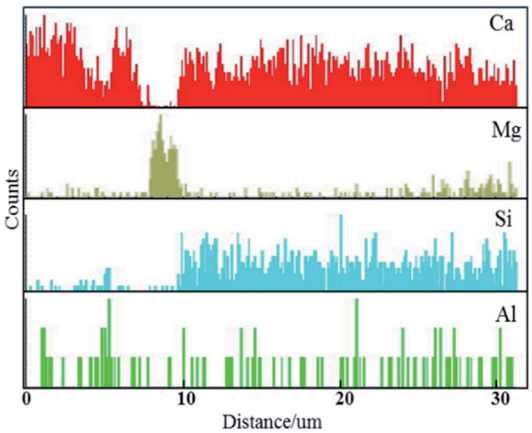

Fig. 3 Line scanning results for the S1 sample at the lime/slag boundary.

Table 2 The composition of product layers at lime/slag boundary slag for the S1 sample (mole, %)

Point	Ca	Si	Mg	Al	O	Phase
1	34.77	3.76	—	—	61.47	CaO
2	2.34	—	48.61	3.20	45.86	MgO
3	31.79	17.02	—	—	51.20	C_2S
4	34.26	16.23	—	—	49.50	C_2S
5	33.83	18.04	—	—	48.13	C_2S
6	25.80	13.52	5.71	2.05	52.96	Slag
7	35.32	18.82	—	—	45.86	Slag (C_2S)

point 2 indicated that a loose product layer of the periclase phase (MgO) was precipitated at the boundary of unmelted lime, and the compositions of point 3–5 indicated that a dense Ca_2SiO_4 (C_2S) layer was formed near the bulk slag.

In order to investigate the effect of the unmelted lime on the existing state of chromium in the stainless steel slag, 5.0% Cr_2O_3 was added into the S2 sample. The SEM backscattered electron images of the product layers at the lime/slag boundary for the S2 sample are shown in Fig. 4. The chemical compositions across the slag/lime boundary analyzed by EDS are given in Table 3. It can be seen from Fig. 4 and Table 3 that two obvious product layers (MgO and C_2S) were observed at the lime/slag boundary. Furthermore, the needle-shaped precipitated phase was found near the unmelted lime, and the needle-shaped precipitated phase could be determined as $CaCr_2O_4$ by the analysis results of both morphology and composition.[13] In addition, according to the binary phase diagram of MgO–$MgCr_2O_4$, $MgCr_2O_4$ can dissolve into MgO at 1873 K, and the periclase phase was a water-soluble phase and prone to dissolve in an aqueous solution. However, the experiment results found that the precipitated periclase phase could dissolve a small amount of Cr, which might pose a great threaten to the environment.[14]

3.2. Formation mechanism of product layers

The isothermal section diagram of the CaO–SiO_2–MgO–4.0% Al_2O_3 slag system shown in Fig. 5 indicated that with the increase in the basicity of slag, the slag phase gradually transformed from the liquid region (L) to the multiphase coexistence region of liquid, dicalcium silicate and periclase phase of 10% (L + C_2S + M). The thermodynamic conditions of the

Table 3 The composition of product layers for S2 sample at the lime/slag boundary (mole, %)

Point	Ca	Si	Mg	Al	Cr	O	Phase
1	36.47	—	—	—	nd[a]	63.53	CaO
2	32.77	—	1.81	—	0.71	64.72	CaO
3	33.64	—	2.07	—	nd[a]	64.29	CaO
4	25.11	—	2.91	2.81	8.58	60.59	Ca–Cr–O
5	16.10	—	—	—	21.46	62.44	$CaCr_2O_4$
6	12.33	—	3.58	1.94	21.46	60.69	$CaCr_2O_4$
7	—	—	42.12	9.77	2.08	46.03	MgO
8	—	—	55.32		3.02	41.66	MgO
9	18.63	9.71	—	—	nd[a]	71.66	C_2S
10	27.06	15.84	—	—	nd[a]	57.10	C_2S
11	22.14	15.08	6.24	2.04	nd[a]	54.50	Slag
12	30.41	15.27	—	—	nd[a]	54.32	C_2S (slag)

[a] nd—not detected.

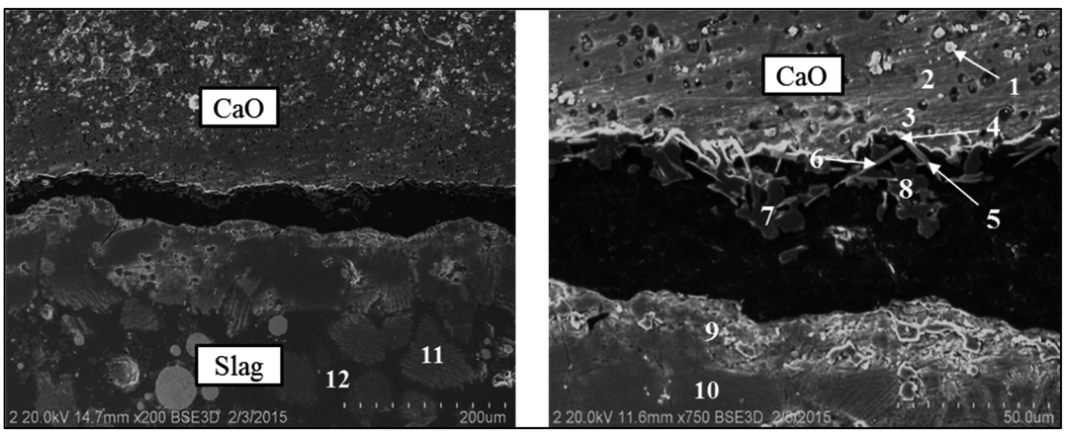

Fig. 4 SEM backscattered electron images for the S2 sample at the lime/slag boundary.

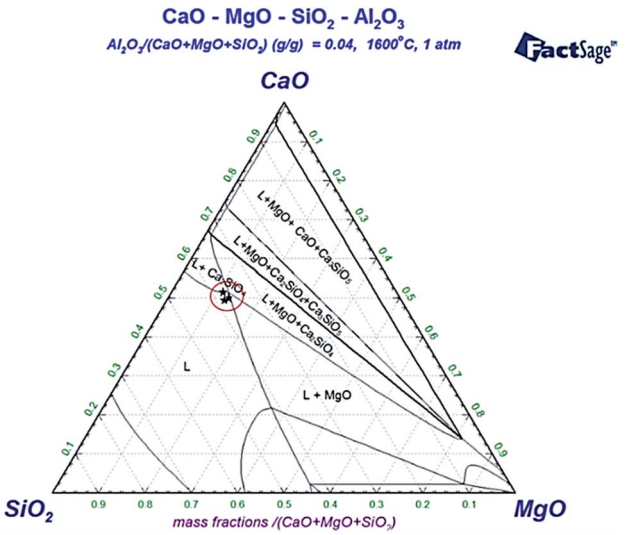

Fig. 5 The $CaO–SiO_2–MgO–Al_2O_3$ phase diagram.

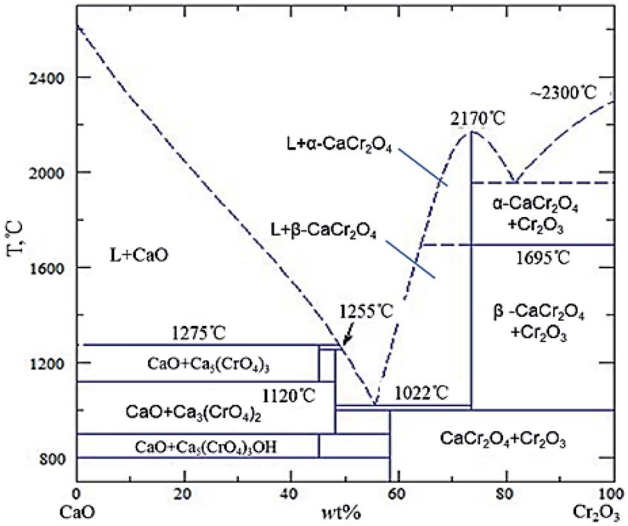

Fig. 6 Phase diagram of $CaO–Cr_2O_3$ in neutral atmosphere.

precipitation of MgO and C_2S phases in the S1 and S2 samples are shown in Table 4. The basicity of the slag in the S1 sample was about 1.3 for the initial precipitation of C_2S. When the basicity of the slag was greater than 1.6, MgO was gradually precipitated from the liquid slag under the saturated state. When 5% Cr_2O_3 was added into the S2 sample, the basicity of slag for the initial precipitation of C_2S and MgO increased to 1.4 and 1.7, respectively. The compositions of the bulk slag marked on the $CaO–SiO_2–MgO–Al_2O_3$ phase diagram shown in Fig. 5 ("★" mark) were not only located at the liquid, MgO and C_2S phase region, but also approached the L + C_2S + M region. This indicated that the liquid phase in the bulk slag near the unmelted CaO was nearly saturated with MgO and C_2S. Fig. 6 shows the binary phase diagram of $CaO–Cr_2O_3$ in a neutral atmosphere. As shown, the $CaCr_2O_4$ phase can stably exist below 2443 K. Therefore, when Cr_2O_3 in the bulk slag diffused to the CaO boundary, $CaCr_2O_4$ could precipitate at the CaO boundary. XRD results shown in Fig. 7 demonstrated that when the CaO block was added into the $CaO–SiO_2–MgO–Al_2O_3–FeO–CaF_2$ slag and $CaO–SiO_2–MgO–Al_2O_3–FeO–CaF_2–Cr_2O_3$ slag, weak peaks of the periclase phase were both found in these slags. Moreover, a small amount of $CaCr_2O_4$ was formed in the chromium-contained stainless steel slag. Related research found that when the basicity of the slag was greater than 2.0, $CaCr_2O_4$ precipitated in the slag,[13] and the precipitated MgO phase dissolved chromium into the solid solution,[15] which verified the reliability of the experimental results in the present study. Therefore, it can be clearly concluded that the unmelted lime in the stainless steel slag can induce the formation of a chromium-contained phase layer at the boundary of lime.

Fig. 8 shows the formation mechanism of product layers at the lime/slag boundary. When the CaO block was added into the molten slag at 1873 K, CaO dissolved gradually from the surface of the CaO block to the bulk slag, resulting in a clear change in the composition of the slag and significant increase in the basicity of the slag. Therefore, MgO and C_2S gradually entered the saturated state, so that MgO and C_2S precipitated at the lime/slag boundary to form the inner and outer product layers, respectively.

The reason for the formation of the structure of the inner and outer product layers (MgO and C_2S) can be explained as follows: based on the $CaO–SiO_2–MgO–Al_2O_3$ phase diagram, C_2S phase easily enters the saturation state. Therefore, the C_2S phase first precipitates around the bulk slag. Afterwards, the MgO phase enters the saturated state and precipitates. In the

Table 4 The basicity of slag with initial precipitation of product layers

Precipitated phase	Initial precipitation basicity of slag	
	S1	S2
Ca_2SiO_4	1.3	1.4
MgO	1.6	1.7

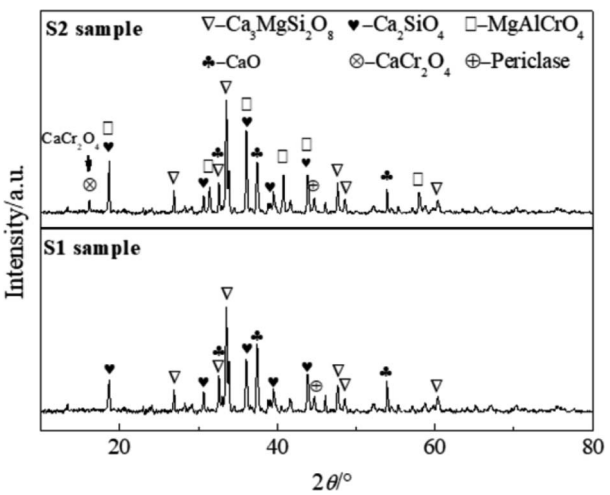

Fig. 7 XRD results of S1 and S2 samples after adding the CaO block.

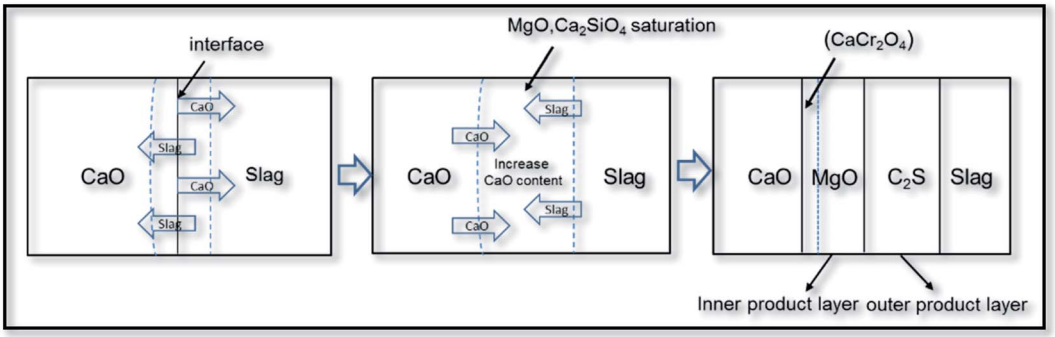

Fig. 8 Formation mechanism of product layers at the lime/slag boundary.

present experiments, it can be found that C_2S was formed in the bulk slag. The chemical potential of the precipitated Ca_2SiO_4 phase of the outer product layer is equal to that of the C_2S phase in the bulk slag, thus the C_2S product layer existed stably near the bulk slag in this study. Simultaneously, MgO could exist stably between CaO and C_2S. Consequently, the MgO product layer existed stably at the lime/bulk slag boundary. Because $CaCr_2O_4$ could only exist stably under high basicity conditions, and the basicity at CaO boundary was high, it was easy to achieve the best thermodynamic conditions for the formation of $CaCr_2O_4$, resulting in the precipitation of needle-shaped $CaCr_2O_4$ at the boundary of the unmelted lime phase.

3.3. Stability of product layers in aqueous solution

The results of element distribution at the lime/slag boundary (Table 3) showed that chromium in the stainless steel slag could be enriched in the MgO and $CaCr_2O_4$ phases at the boundary of the unmelted lime. In order to gain a better understanding of the solubility of MgO and $CaCr_2O_4$ in an aqueous solution, the Pourbaix diagrams of Mg–H_2O and Ca–Cr–H_2O systems at 298 K were calculated, and are shown in Fig. 9(a) and (b). The molality of all the aqueous species in these systems was fixed at 1. It can be seen from Fig. 9(a) that the MgO phase may exist stably with $Mg(OH)_2$ in the alkaline solution. However, when the pH of the aqueous solution is less than 8, MgO becomes gradually unstable in an aqueous solution. Therefore, the MgO phase is unstable in a weak acid solution, which might enhance the leaching of chromium under environmental conditions. The potential–pH diagram of the Ca–Cr–H_2O system (Fig. 9(b)) indicates that $CaCr_2O_4$ is unstable in a weakly acidic aqueous solution, and $CaCr_2O_4$ transforms to Ca^{2+} and $Cr(OH)^{2+}$ as the pH is less than 6, and to Ca^{2+} and Cr^{3+} at pH < 4. Furthermore, when the CaO–Cr_2O_3 binary oxides were soaked in air atmosphere below 1501 K, it was conducive to the formation of the compounds containing Cr^{6+} ($CaCrO_4$), as described in eqn (1).[16] Lee Y. *et al.* reported that the presence of unmelted lime in stainless steel slag was in favor of the generation of $CaCrO_4$.[17,18] When the slag was heated at 773–1273 K, the amount of Cr^{6+} clearly increased, and the elution of chromium was improved. It can be also found from Fig. 9(b) that $CaCrO_4$ is not stable in the aqueous solution in the wide pH range. In addition, the f-CaO in steel slag can react with water to produce $Ca(OH)_2$, which causes volume expansion and dust generation.[19,20] The escaping dust may release Cr^{6+} into the environment, thereby causing harm to humans. As stated above, the unmelted lime may have great effect on the application security of the stainless steel slag.

$$\tfrac{1}{2}CaO + \tfrac{1}{2}\beta Cr_2O_4 + \tfrac{3}{4}O_2 \rightarrow CaCrO_4,\ \Delta G^{\ominus} = -191\,250 + 109T\ (J\ mol^{-1}) \quad (1)$$

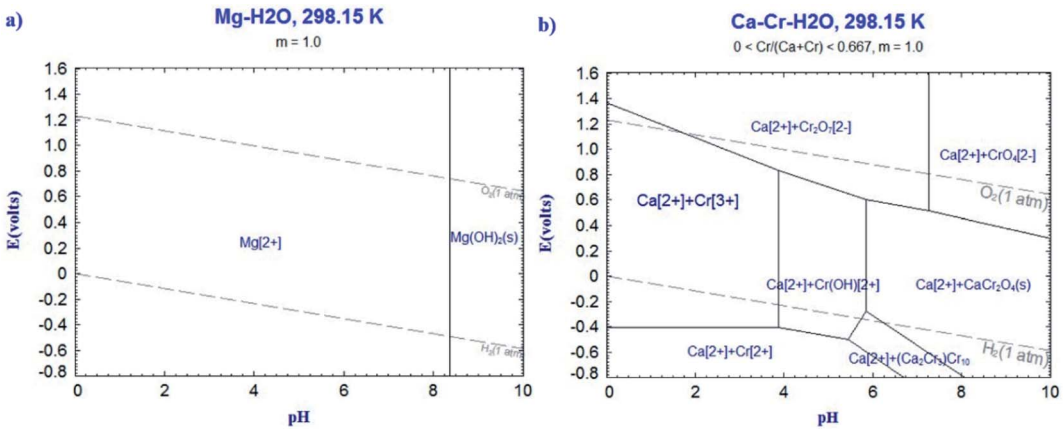

Fig. 9 The potential–pH diagrams at 298 K, (a) Mg–H_2O system, (b) Ca–Cr–H_2O system.

The leaching experiment results (ICP-OES results) showed that when the stainless steel slag contained the unmelted lime phase, the leaching content of chromium in the slag was 2.08 mg L^{-1}, which was much higher than the leaching content of chromium of 0.62 mg L^{-1} in the slag without the unmelted lime phase.

4. Conclusions

In this study, the influences of unmelted lime on the structure of product layers at the lime/slag boundary and the existing state of chromium oxide in CaO–SiO_2–Al_2O_3–MgO–FeO–CaF_2–(Cr_2O_3) slags were investigated by scanning electron microscope-energy dispersive spectroscopy (SEM-EDS) and FactSage 7.1. The results indicated that after adding the CaO block for 20 min, MgO and Ca_2SiO_4 two different product layers were formed at the boundary between the unmelted lime and the bulk slag in the CaO–SiO_2–Al_2O_3–MgO–FeO–CaF_2 slag, which indirectly restricted the dissolution of CaO. The thickness of the MgO layer near the unmelted lime was approximately 10 μm, and the thickness of the Ca_2SiO_4 layer near the bulk slag was 60–80 μm. When the unmelted CaO existed in the CaO–SiO_2–Al_2O_3–MgO–FeO–CaF_2–Cr_2O_3 stainless steel slag, besides the MgO and Ca_2SiO_4 product layers, a needle-shaped $CaCr_2O_4$ phase also precipitated at the boundary of the unmelted lime. Moreover, a small amount of Cr element can dissolve into MgO. The Eh–pH diagrams show that both $CaCr_2O_4$ and MgO phases unstably existed in the weak acid aqueous solution; thus, the presence of unmelted lime in the stainless steel slag can enhance the leachability of chromium.

Conflicts of interest

No potential conflict of interest was reported by the authors.

Acknowledgements

This work was supported by the Natural Science Foundation Youth Fund Project of Shandong Province (ZR2020QE145).

References

1 D. Rai, B. M. Sass and D. A. Moore, *Inorg. Chem.*, 1987, **26**, 345.
2 K. Pillay, H. V. Blottnitz and J. Petersen, *Chemosphere*, 2003, **52**, 1771.
3 Y. A. Samad, T. Miki and M. Hino, *ISIJ Int.*, 2011, **51**, 728.
4 H. Suito and R. Inoue, *ISIJ Int.*, 2006, **46**, 180.
5 X. Yang, H. Matsuura and S. F. Tsukihashi, *ISIJ Int.*, 2009, **49**, 1298.
6 T. Hamano, S. Fukagai and F. Tsukihashi, *ISIJ Int.*, 2006, **46**, 490.
7 T. Deng, J. Gran and S. C. Du, *Steel Res. Int.*, 2010, **81**, 347.
8 Z. S. Li, M. Whitwood, S. Millman and J. V. Boggelen, *Ironmak. Steelmak.*, 2014, **41**, 112.
9 H. W. Kilau and I. D. Shah, *Preventing chromium leaching from waste slag exposed to simulated acid precipitation: A Laboratory Study*, US, 1984.
10 H. Cabrera-Real, A. Romero-Serrano, B. Zeifert, A. Hernandez-Ramirez, M. Hallen-Lopez and A. Cruz-Ramirez, *J. Mater. Cycles Waste Manage.*, 2012, **14**, 317.
11 V. Arredondo-Torres, A. Romero-Serrano, B. Zeifert and J. Cruz-Rivera, *Rev. Metal. Madrid*, 2006, **42**, 417.
12 P. Drissen, A. Ehrenberg, M. Kühn and D. Mudersbach, *Steel Res. Int.*, 2009, **80**, 737.
13 J. Burja, F. Tehovnik, J. Medved, M. Godec and M. Knap, *Mater. Tehnol.*, 2014, **48**, 753.
14 A. M. Alper, R. N. Mcnally, R. C. Doman and F. G. Keihn, *J. Am. Ceram. Soc.*, 1964, **47**, 30.
15 L. H. Cao, C. J. Liu, Q. Zhao and M. F. Jiang, *J. Iron Steel Res. Int.*, 2017, **24**, 258.
16 A. Yamaguchi, *China's Refractories*, 2007, **16**, 3.
17 Y. Lee and C. L. Nassaralla, *Metall. Mater. Trans. B*, 1997, **28**, 855.
18 Y. Lee and C. L. Nassaralla, *Metall. Mater. Trans. B*, 1998, **29**, 405.
19 W. P. Yin, *Res. Iron Steel*, 2010, **38**, 24.
20 W. J. Tang, H. Q. Liao, Y. Zhou, W. J. Zhao and H. H. Chen, *Steelmak.*, 2009, **25**, 34.